International Journal of Engineering Research & Technology (IJERT)
ISSN: 2278-0181
Vol. 4 Issue 04, April-2015

Nonlinear Behavior of Reinforced Concrete Continuous Deep Beam

Wissam D. Salman
Lecturer Doctor,
Department of Civil Engineering,
DiyalaUniversity,Baqubah, Iraq

***Abstract*— This paper presents numerical investigation of nine continuous reinforced concrete deep beams were experimentally tested and collected from literature. The collected specimens cover several parameters which usually influenced on strength and behavior of continuous deep beams as shear span to depth ratio, the reinforcement ratio, the effective depth, and the concrete compressive strength. All beams had the same longitudinal top and bottom reinforcement and no web reinforcement to assess the effect of changing the beam depth on the shear strength of such beams. A three-dimensional finite element model using (ANSYS 12) program is used.**
It was found that the general behaviors through the linear and nonlinear ranges up to failure of the finite elements model show good agreement with observations and data from the experimental beam tests.

Keywords—Continuous deep beams; Finite element; Ansys.

1. INTRODUCTION

Reinforced concrete continuous deep beams are fairly common structural elements. They are characterised as being relatively short and deep, having a small thickness relative to their span or depth. Typical applications of deep beams include transfer girders, pile caps, tanks, folded plates and foundation walls, often receiving many small loads in their own plane and transferring them to a small number of reaction points. Elastic solutions of reinforced concrete deep beams provide a good description of the behavior before cracking, but after cracking, a major redistribution of stresses occurs and hence the beam capacity must be predicted by inelastic analysis [1].
Due to this small ratio (i.e. shear span to depth ratio) the behavior differs in various ways from the normal beam behavior. In construct to slender beams, the response of deep beams is characterised by a significant direct load transfer from the point of loading to the supports, and a nonlinear strain distribution over the depth of the cross section (even in elastic stage). The deformations by shear are not negligible any more, compared to those caused by flexure furthermore the large stiffness of this type of structures makes them highly sensitive to differences in support settlements [2].

2. LITERATURE REVIEW

Sultan [3] used the results of testing 261 deep beams, 106 of which were without reinforcement and the others with vertical or horizontal stirrups or both. The main variables were the shear span to depth ratio (a/d), longitudinal reinforcement ratio, concrete compressive strength and vertical and horizontal web shear stress reinforcement. Test results showed that, for beams with $a/d \leq 2.5$, these variables had a significant effect on the ultimate shear strength of these beams. It was also found that the ultimate shear strength increases significantly with increasing concrete compressive strength and longitudinal reinforcement ratio, and with decreasing shear span to effective depth ratio.

Samir M. O., Dirar and Chris T. Morley [4] describes a series of nonlinear finite element analyses carried out using the commercial package, DIANA7 to predict the ultimate load and mode of failure for three different types of reinforced concrete continuous two-span deep beams. Only one parameter, the shear retention factor, was varied during the analysis. They concluded that the finite element method is capable of modeling the behavior of the reinforced concrete deep beams, and the predictions of the ultimate load are within an accuracy region of 5%.

Lee J. K, Li C. G. and Lee Y.T. [5] tested RC continuous deep beams to evaluate the shear strength with various location of web opening, in total five specimens with circular web opening have been cast and tested in the laboratory it has been observed that the specimens with web opening have about 90% of shear strength of the specimen without web opening, in general the span with web opening is less stiff than have the span without web opening. Web opening in the deep beam with shear span to depth ratio of 1.0 can be located not in the compressive strut area but tensile area in this case adequate reinforcement should be provided around the opening to avoid the crack width wider and fail and the shear strength of deep beams with web opening whose diameter is 0.3 times of depth is (87 to 92%) of rest result of deep beam without opening

Ashour A. F. and Morley C. T. [6] carried out an upper bound mechanism analysis on continuous reinforced concrete deep beams. The effect of horizontal and vertical web reinforcement on the load carrying capacity is mainly influenced by the shear span to-effective depth ratio. In deep beams, the horizontal shear reinforcement is effective than the vertical shear reinforcement.

Leonhardt F. and Walther R. [7] tested two reinforced continuous deep beams, both of which failed in shear at their interior shear spans. The test results showed that the distributions of bending moments and support reactions in continuous concrete deep beams were substantially different from those in continuous shallow beams.

Rogowsky D.M., Mac Gregor J.G., and Ong S.Y. [8] tested seven simply supported and seventeen two span deep beams under concentrated loads. The tested specimens are divided into three series of similar shear span to depth ratio. Typical series consisted of seven beams having different reinforcement patterns. They concluded that the behavior ranged from brittle for beams without vertical web reinforcement to ductile for beams with large amount of vertical web reinforcement. The

horizontal web reinforcement has no effect on the ultimate capacity.

3. EXPERIMENTAL TECHNIQUE

3.1 CHARACTERISTICS OF TESTED DEEP BEAMS

Nine continuous reinforced concrete deep beams were collected from literature [9]. They were constructed and tested to failure. The objective of the test program was to show the influence of section depth on the structural behavior and ultimate strength of continuous deep beams. The details of geometrical dimensions and reinforcement for test specimens are shown in Table (1) and Figure (1). Main variables investigated were beam depth (h), ranged from 400 mm to 720 mm, compressive strength of concrete, f'_c, and shear span-to-overall depth ratio, a/h. The beams tested were classified into two groups according to the concrete compressive strength: L-series for concrete with low compressive strength and H-series for concrete with high compressive strength. The shear span-to-overall depth ratios, a/h, were initially designed to be 0.5 to 1.

All tested beams had the same section width and longitudinal reinforcement ratio: the section width, b_w, was 160 mm and longitudinal top and bottom reinforcement ratios were about 1%. The total length of test specimens varied according to the a/h ratio as given in Table (1). The distance between the soffit of beams and centre of longitudinal reinforcement was 45 mm for beams having section depths of 400 mm and 600 mm, and 67 mm for beams with section depth of 720 mm.

The longitudinal bottom reinforcement was continuous over the full length of the beam and welded to 160×100×10 mm end plates to provide sufficient anchorage. The longitudinal top reinforcement was anchored within the outside of exterior supports by 90° hooks as shown in Figure (1). To examine the influence of the size effect on concrete continuous deep beams, no shear reinforcement was provided.

Table 1 Details of continuous reinforced concrete deep beams [9]

Specimen	f'_c	a/h	h (mm)	a (mm)	d (mm)	L (mm)	$A_{st} = A'_{st}$ (mm^2)	$\rho_s = \rho'_s$
L5–40	32.4	0.5	400	200	355	400	574	0.01
L5–60	32.4	0.5	600	300	555	600	861	0.0097
L5–72	32.4	0.5	720	360	653	720	1148	0.011
L10–40	32.1	1.0	400	400	355	800	574	0.01
L10–60	32.1	1.0	600	600	555	1200	861	0.0097
L10–72	32.1	1.0	720	720	653	1440	1148	0.011
H6–40	65.1	0.6	400	240	355	480	574	0.01
H6–60	65.1	0.6	600	360	555	720	861	0.0097
H6–72	65.1	0.6	720	432	653	864	1148	0.011

Note: f'_c=cylinder compressive strength , a/h = shear span-to-overall depth ratio, h = section overall depth, a = shear span, d=effective section depth, L=beam span , A_{st} = total area of longitudinal bottom reinforcement , A'_{st} = total area of longitudinal top reinforcement, ρ_s=longitudinal bottom reinforcement ratio (A_{st}/ bwd), ρ'_s =longitudinal top reinforcement ratio (A'_{st}/bwd) and bw=beam width.

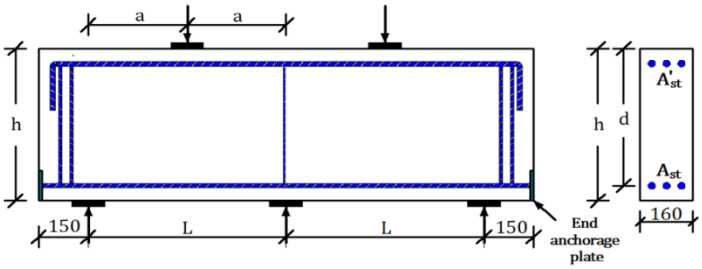

Figure (1) Details of beam geometry and arrangement of reinforcements [9]

4. FINITE ELEMENT MODELS

The general purpose FE software ANSYS (ANSYS, 2012) was employed to generate FE models to simulate numerically the structural response of the previously described continuous reinforced concrete deep beams [9]. The generated models were validated against all respective experimental results.

4.1 ELEMENT TYPES

4.1.1 SOLID 65 ELEMENT DESCRIPTION

SOLID 65 (or 3-D reinforced concrete solid) is used for the 3-D modeling of solids with or without reinforcing bars (rebar). The geometry and node location for this element type are shown in Figure (2). The solid is capable of cracking in tension and crushing in compression. In concrete applications, for example, the solid capability of the element may be used to model the concrete, while the rebar capability is available for modeling reinforcement behavior. Other cases for which the element is also applicable would be reinforced composites (such as fiberglass), and geological materials (such as rock). The element is defined by eight nodes having three degrees of freedom at each node: translations of the nodes in x, y, and z-directions. Up to three different rebar specifications may be defined [10].

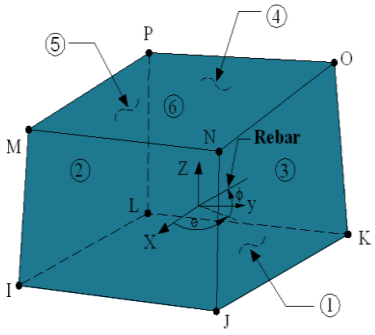

Figure (2) Element (SOLID65) geometry [10]

4.1.2 SOLID 45 ELEMENT DESCRIPTION

An eight node solid element, SOLID45, was used for steel supports in the beam models. The element is defined with eight nodes having three degrees of freedom at each node translations in x, y and z directions [10]. The geometry and node location for this element type are shown in Figure (3). Steel plates were added at support and point of loading

locations in the finite element models (as in the actual beams) to provide a more even stress distribution over the support and point of loading areas. An elastic modulus equal to 200000 MPa and Poisson's ratio of 0.3 were used for the plates. The steel plates were assumed to be linear elastic materials.

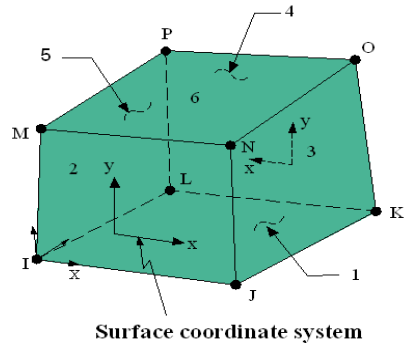

Figure (3) Element (SOLID45) geometry [10]

4.1.3 LINKE 8 ELEMENT DESCRIPTION

LINK8 is a spar (or truss) element which may be used in a variety of engineering applications. This element can be used to model trusses, sagging cables, links, springs, etc. The 3-D spar element is a uniaxial tension-compression element with three degrees of freedom at each node: translations of the nodes in x, y, and z-directions. As in a pin-jointed structure, no bending of the element is considered. Plasticity, creep, swelling, stress stiffening, and large deflection capabilities are included. This element is used, in this study, to simulate the behavior of steel reinforcement which works as main steel reinforcement in resisting the flexural stresses. The geometry, node locations, and the coordinate system for this element are shown in Figure (4) [10].

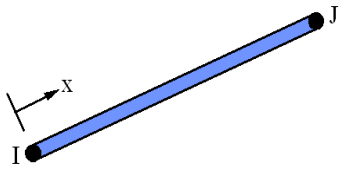

Figure (4) Element (LINK8) geometry [10]

4.2 MATERIALS MODELING

4.2.1 CONCRETE

The ANSYS program requires the uniaxial stress-strain relationship for concrete in compression. The adopted compressive uniaxial stress-strain relationship for concrete is the multi-linear isotropic stress-strain curve shown in Figure (5), and calculated by the relations [11]:

$$f_c = \varepsilon E_c \quad \text{for} \quad 0 \le \varepsilon \le \varepsilon_1 \qquad (1)$$

$$f_c = \frac{\varepsilon\, E_c}{1 + \left(\frac{\varepsilon}{\varepsilon_\circ}\right)^2} \quad \text{for} \quad \varepsilon_1 \le \varepsilon \le \varepsilon_\circ \qquad (2)$$

$$f_c = f_c' \quad \text{for} \quad \varepsilon_\circ \le \varepsilon \le \varepsilon_{cu} \qquad (3)$$

and

$$\varepsilon_1 = \frac{0.3\, f_c'}{E_c} \qquad (4)$$

$$\varepsilon_\circ = \frac{2\, f_c'}{E_c} \qquad (5)$$

Where: ε_1 = strain corresponding to $(0.3 f_c')$, $\varepsilon_\circ$ =strain at peck point, ε_{cu}= ultimate compressive strain.

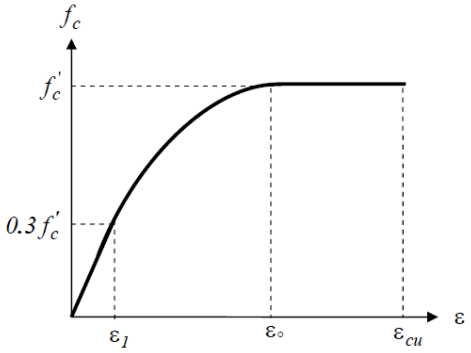

Figure (5) Multi-linear compressive uniaxial stress-strain curve for concrete [11]

Other parameters required to perform the finite element analysis are the shear transfer coefficients. These coefficients range from 0.0 to 1.0, with 0.0 representing a smooth crack (complete loss of shear transfer) and 1.0 representing a rough crack (no loss of shear transfer). This specification may be made for both the closed and open crack. When the element is cracked or crushed, a small amount of stiffness is added to the element for numerical stability (ANSYS 12.1). The Poisson ratio for concrete is usually taken as 0.2 [12]. The modulus of elasticity (E_c), and the modulus of rupture (f_r) for concrete (which are required in the ANSYS 12.1analysis) are both calculated by equations (6) and (7), according to the ACI 318-08 specifications [13] (units MPa):

$$E_c = 4700\sqrt{f_c'} \qquad (6)$$

$$f_r = 0.62\sqrt{f_c'} \qquad (7)$$

4.2.2 STEEL REINFORCEMENT AND STEEL PLATES

Steel is a much simpler material to represent. Its stress- strain behavior can be assumed to be identical in tension and in compression. A typical uniaxial stress-strain curve for a steel specimen loaded monotonically in tension is shown in Figure (6).

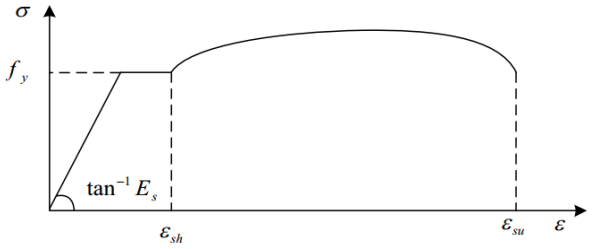

Figure (6) Typical stress-strain curve for steel [14]

The stress-strain diagram may for simplicity consist of two branches: the first branch starts from the origin with a slope equal to E_s up to f_y. A second branch is horizontal or, for practical use of computers, is assumed to have a very small slope such as $10^{-4}E_s$ and this last case is limited to the strain 0.01 according to Euro-code [15].

4.3 MESHING

In order to obtain accurate results from the FE model, all the elements in the model were purposely assigned the same mesh size to ensure that each two different materials share the same node. Figure (7) shows the typical mesh of the FE model of continuous deep beam specimens. Modeling and mesh generation is developed using same techniques for all specimens.

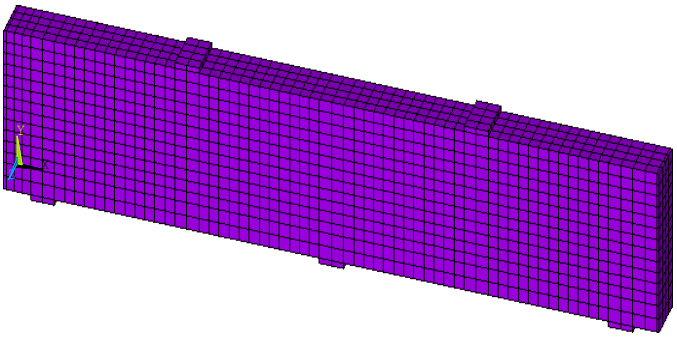

Figure (7) Meshing of continuous concrete deep beam

4.4 BOUNDARY CONDITIONS AND LOADING

The boundary conditions for the models created with 3D solid elements representing the supporting plates are defined as follows: pin support: the nodes along the transverse line at the middle bottom of the supporting plate were locked against translation in all directions vertical (y-direction), transverse (x-direction) and longitudinal (z-direction). Roller support: The nodes along the transverse line at the middle bottom of the supporting plate were locked against translation in only one vertical direction (y-direction). The loading profile is applied to the model. The loading plate serves as a medium that uniformly distributes the pressure on the loaded area. For finite element model loading, and defined boundary conditions can be seen in Figure (8).

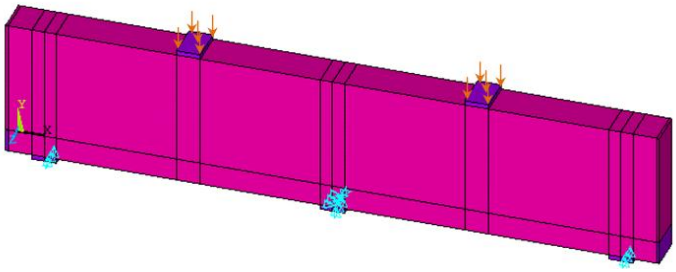

Figure (8) Loading profile and boundary conditions

5. NUMERICAL ANALYSIS: VERIFICATION OF FINITE ELEMENT MODEL

5.1 LOAD-DEFLECTION RESPONSES

To verify the proposed finite element model, a comparison of load–midspan deflection response acquired from test results is demonstrated. The comparison between experimental and the numerical load-deflection curves for the mid span deflection of the continuous deep beams are shown in Figure (9). It shows that the finite element load deflection curves are somewhat stiffer than the experimental plots. After first cracking, the stiffness of the finite element models is again higher than that of the experimental beams. There are several effects that may cause the higher stiffness in the finite element models. The most important is micro cracks which are present in the concrete for the experimental deep beams, and could be produced by drying shrinkage in the concrete and/or handling of the deep beams. On the other hand, the finite element models do not include the micro cracks. As well known that the micro cracks reduce the stiffness of the experimental deep beams. For all specimens, good agreement is in load-deflection relation prior to failure load. For each of the test deep beams, the predicted and the measured maximum loads were in good agreement. The values given by all specimens were similar to the analytical results; comparative data are summarized in Table (2). The mean ratios of experimental-to-numerical ultimate load (predicted by ANSYS) were 1.04. In general, the load-deflection curve from the experiment and the FEM analysis were in very good agreement.

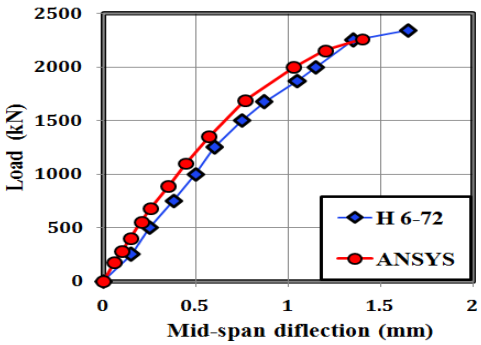

Figure (9) FE versus experimental load-deflection curves of the studied continuous deep beams, cont,d

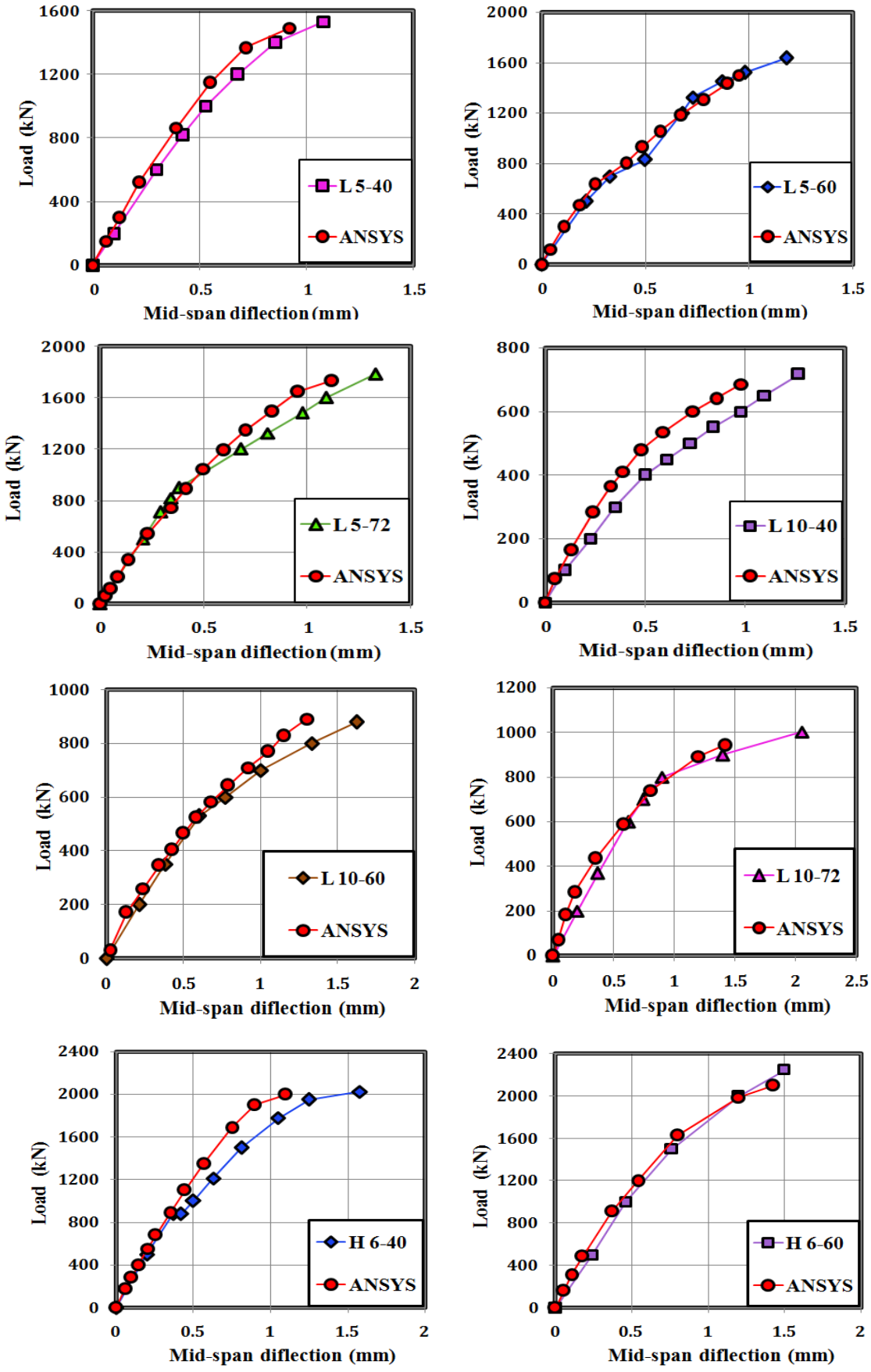

Figure (9) FE versus experimental load-deflection curves of the studied continuous deep beams

Table (2) Experimental and predicted ultimate load capacity (Pu) of continuous deep beams

Specimen	P_u (kN) Experimental	P_u (kN) ANSYS	$P_{u_{Exp.}}/P_{u_{ANS.}}$
L5–40	1529	1490.2	1.02
L5–60	1635	1496.8	1.09
L5–72	1786	1733.5	1.03
L10–40	717	685.8	1.05
L10–60	880	892	0.98
L10–72	1003	943.3	1.06
H6–40	2025	1997	1.01
H6–60	2248	2100	1.07
H6–72	2342	2262	1.04
Mean			1.04

5.2 DIAGONAL CRACKING AND FAILURE MODE

The crack patterns of the beams at their respective peak loads are shown in Figure (10). The crack patterns in this Figure indicate that the beams fail in the same manner. Although the crack patterns given in Figure (10) are in smeared form, it can be seen that the overall crack patterns obtained by the finite element analysis coincide quite closely with the test observation that when the applied load reached the peak, a major diagonal crack in the intermediate shear span ran between the edges of the applied load and the intermediate support plates.

The failure modes and crack pattern in H-series were similar to those in L-series but lager failure zone [9]. Just before failure, the two spans showed nearly the same crack patterns. The crack pattern development was significantly influenced by both a/h ratio and section depth. For $a/h = 0.5$, the first diagonal crack developed at the mid-depth of the concrete strut within the interior shear span, and then the first flexural crack in the sagging region immediately followed. As the load increased, more flexural and diagonal cracks were formed and a diagonal crack extended to join the edges of the load and intermediate support plates. A diagonal crack within the exterior shear span occurred near to the failure load.

For beams having $a/h = 1.0$, the first crack developed vertically in the hogging zone, followed by a diagonal crack in the interior shear span and then a vertical crack in the sagging zone. Diagonal cracks within the exterior shear span are seldom developed, exhibiting different crack patterns from that observed in beams with $a/h = 0.5$,.

With the increase of h, the number of cracks formed decreased. Bazant et al. [16] mentioned that the number of cracks decreased and their depth was also reduced with the increase of h because of the increase of the energy release rate and expansion of crack width, which caused brittle failure.

All beams exhibited the same mode of failure. At failure, an end block formed because of the significant diagonal crack connecting the edges of the load and intermediate support plates and rotated about the exterior support. The observed failure mode suggests that the mechanism analysis, appears very promising in predicting the load capacity of such beams.

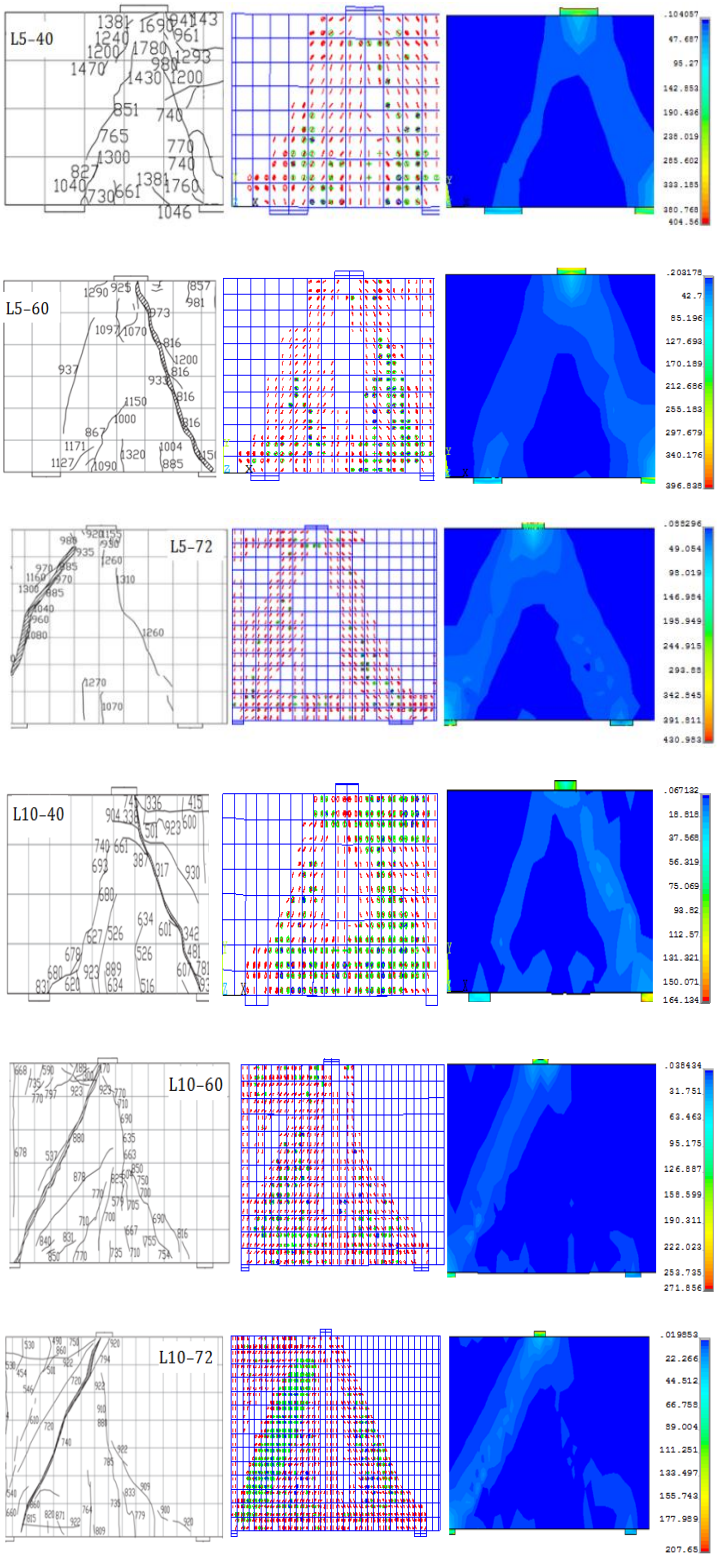

Figure (5) Crack patterns and failure mode in L-series beams

6. CONCLUTIONS

In this paper, the nonlinear finite element analysis by ANSYS was used to predict the behavior and strength of continuous reinforced concrete deep beams. The agreement between the

numerical simulations and experimental findings demonstrate the overall accuracy and reliability of the analytical models in predicting the response of that this new type of structural elements. Based on the results of the numerical simulations and comparisons with experimental data, the following conclusions were reached:

1. The results from the finite element simulation agree very well with the experimental observations, especially with regards to load-deflection response, crack patterns, failure modes and mechanisms. All these indicate that the constitutive models used for beam materials able to capture the fracture behavior of continuous reinforced deep beam accurately. Consequently, this method may be used for the nonlinear analysis and design of such elements very efficiently.
2. In general, the experiment results of continuous reinforced concrete deep beams and the FEM analysis by ANSYS were in very good agreement. The mean ratios of experimental to predicted values for ultimate load capacities equal 1.04.
3. ANSYS can monitor and capture the shape and propagation of cracks during loading till failure. The predictions of the failure modes of all the beams by finite element agree well with the experimental observations.

7. REFERENCES

[1] Ashour A. F. and Yang K. H., "Application of Plasticity Theory to Reinforced Concrete Deep Beams: A Review", Magazine of Concrete Research, Vol. 60, No. 9, PP. 657-664, November, 2008.
[2] Asin M., "The Behavior of Reinforced Concrete Continuous Deep Beams", MSc Thiess, Delft University, 2000.
[3] Sultan A. A., “Shear Capacity of Reinforced Concrete Deep Beams”, MSc Thesis, University of Technology, Baghdad, Iraq, PP.110, 2003.
[4] Samir M. O., Dirar and Chris T. Morley, "Nonlinear Finite Element Analysis of Reinforced Concrete Deep Beams", International Conference on Computational Plasticity, Barcelona, 2005.
[5] Lee J. K, Li C. G. and Lee Y.T., "Experimental Study on Shear Strength of Reinforced Concrete Continuous Deep Beams with Web Opening", The 14th World Conference on Earthquake Engineering, 2008.
[6] Ashour A. F. and Morley C. T., "Effectiveness Factor of Concrete in Continuous Deep Beams", ASCE, Journal of Structural Engineering, Vol. 122, No. 2, PP. 169-178, February, 1996.
[7] Leonhardt F. and Walther R., "Wandartige Trager (Deep Beams)." Deutscher Ausschuss Für Stahlbeton Bull. ,Wilhelm Ernst and Sohn, Berlin, Germany (in German), 1966.
[8] Rogowsky D.M., Mac Gregor J.G. and Ong S.Y.," Test of Reinforced Concrete Deep Beams", ACI Journal, Vol. 83, No. 4, PP. 614-623, July-Aug., 1986.
[9] Yang K. H., Chung H. S. and Ashour A. F., “Influence of Section Depth on the Structural Behavior of Reinforced Concrete Continuous Deep Beams”, Magazine of Concrete Research, Vol. 59, No. 8, PP. 575–586, 2007.
[10] ANSYS, ANSYS User’s Manual Revision 12.1, ANSYS, Inc., Canonsburg, Pennsylvania, 2012.
[11] Desayi P. and Krishnan S., “Equation for the Stress-Strain Curve of Concrete”, Journal of the American Concrete Institute, Vol. 61, No. 3, PP. 345-350, March, 1964.
[12] Bandara H. R. C. S., Gamage J. C. P. H., Aravinda M. D., and Weerakon S. D., "FE Modeling of CFRP Strengthened Concrete Beam Exposed to Cyclic Temperature, Humidity and Sustained Loading”, Civil Engineering Research for Industry , Department of Civil Engineering, University of Moratuwa, PP. 55-60, 2011.
[13] ACI 318-08, American Concrete Institute, “Building Code Requirements for Reinforced Concrete,” American Concrete Institute, Farmington Hills, Michigan, 2008.
[14] Chen W.F. "A plasticity in Reinforced Concrete", First Edition, J. Ross publishing, Inc., copyright, 2007.
[15] European Committee for Standardisation (CEN), Eurocode 4, "Design of Composite Steel and Concrete Structures", Part 1.1: General Rules and Rules for Buildings, DD ENV, 1994.
[16] Bazant Z. P. and Planas J., "Fracture and Size Effect in Concrete and Other Quasi Brittle Materials", CRC Press, Boca Raton, Florida, 1998.